

Hirshfeld surface, spectroscopic investigation (FT-IR, Raman and NMR), reactive descriptor and docking study of naphthalene-1-yl acetic acid

M. Kavimani¹, V. Balachandran¹, B. Narayana², K. Vanasundari¹ and B. Revathi¹

¹Centre for Research-Department of Physics, Arignar Anna Govt. Arts College, Musiri, Tiruchirappalli-621 211, India.

²Department of Studies in Chemistry, Mangalore University, Mangalagangothri-574 199, India.

ARTICLE INFO

Article history:

Received: 04 July 2017;

Received in revised form:

8 August 2017;

Accepted: 18 August 2017;

Keywords

Vibrational spectra,
HOMO-LUMO,
NBO,
Hirshfeld,
Docking.

ABSTRACT

The Fourier transform infrared, FT-Raman and NMR spectra of Naphthalene-1-yl acetic acid (NAA) have been recorded and analyzed. Harmonic vibrational frequencies have been investigated with the help of Density functional theory (DFT) with 6-31+G(d, p) and 6-31++G(2d, 2p) basis sets. The Gauge-Invariant Atomic Orbital Approach (GIOA) is used to calculate the proton and carbon chemical shifts of the title compound. The natural bond orbital analysis of the title compound is also reported in order to understand the stability of the molecule which arises from hyper-conjugative intermolecular interactions and charge delocalization. The polarizability (α), first order hyper-polarizability (β) and second order hyper-polarizability (γ) values of the investigated molecule have been computed using DFT quantum mechanical calculations. The molecular orbital contributions are studied by density of energy states (DOSs). The reactivity sites are by mapping the electron density into electrostatic potential surface (MEP). Mulliken analysis of atomic charges is also calculated. The electron density-based local reactivity descriptors such as Fukui functions were calculated to explain the chemical selectivity or reactivity site in NAA. Hirshfeld surface and fingerprint plots reveal that the complex structure is stabilized mainly by H...H, C...C, C...H intermolecular interactions. Finally molecular docking studies have been carried out in the active site of NAA was also investigated.

© 2017 Elixir All rights reserved.

1. Introduction

Naphthalene and its derivatives are widely used as the chemical intermediate wetting agent in many industrial applications, to study heat transfer with mass sublimation in the engineering field, household fumigants such as mothballs, fumigant pesticides. Naphthalene and alkylated naphthalenes are semi-volatile, present in the atmosphere much in the gas-phase [1]. NAA is an organic compound with the formula $C_{10}H_7CH_2CO_2H$. This colorless solid is soluble in organic solvents. It features a carboxymethyl group (CH_2CO_2H) linked to the "1st-position" of naphthalene. NAA is a synthetic plant hormone in the auxin family and is an ingredient in many commercial plants rooting horticultural products; it is a rooting agent and used for the vegetative propagation of plants from stem and leaf-cutting. It is also used for plant tissue culture [2]. The hormone NAA does not occur naturally and like all auxins is toxic to plants at high concentrations. In the United States, under the Federal Insecticide, Fungicide, and Rodenticide Act (FIFRA), products containing NAA require registration with the Environmental Protection Agency (EPA) as pesticides.

NAA is widely used in agriculture for various purposes. It is considered to be only slightly toxic but when at higher concentrations it can be more toxic to animals. This was shown when tested on rats via oral injection the quantity of NAA at 1000–5900 mg/kg, to inject the rat it is a very toxic level to the rat. So NAA has a toxic one to animals [3]. NAA has been shown to greatly increase cellulose fiber formation in

plants when paired with another phytohormone called gibberellic acid. Because it is in the auxin family it has also been understood to prevent premature dropping and thinning of fruits from stems. Increased amounts of it can actually have negative effects however and cause growth inhibition to the development of plant crops. It has been used on many different crops including apples, olives, oranges, potatoes, and various other hanging fruits. In order for it to obtain its desired effects, it must be applied in concentrations ranging from 20–100 $\mu\text{g/mL}$ [4]. NAA is present in the environment undergoes oxidation reactions with hydroxyl radicals and sulphate radicals. Radical reactions of NAA were studied by using pulse radiolysis technique. Hydroxyl adduct radical was formed as the intermediate during the reaction of hydroxyl radical with NAA. The intermediate naphthyl methyl radical was formed during the reaction of sulphate radical anion with NAA[5].

In the micro propagation of various plants, NAA is typically added to a media containing nutrients essential to the plant's survival. It is added to help induce root formation in various plant types. It can also be applied by spraying it on to plants and which is typical in agricultural use. It is prohibited in many areas to use it in high concentrations due to the health concerns towards humans and other animals.

In this work, structural parameters, vibrational assignments, electronic absorption and frontier molecular orbital energies are calculated for NAA.

Due to the different potential biological activity of the title compound, molecular docking was also reported.

2. Experimental details

The FT-IR spectrum of the molecule is recorded in the region 4000-400 cm^{-1} in Perkin Elmer FT-IR spectrometer. The FT-Raman spectrum of the sample is recorded using 1064 nm line of Nd:YAG laser as excitation wavelength in the region 4000-0 cm^{-1} on a Bruker RFS 66 V FT-Raman spectrometer. The detector is a liquid nitrogen cooled Ge detector.

NMR spectrum is performed in Bruker DPX 600 MHz at 300 K. The compound is dissolved in DMSO and the chemical shifts are reported in ppm relative to tetramethylsilane (TMS) for ^1H and ^{13}C NMR spectra. ^1H and ^{13}C NMR spectra are obtained at a base frequency of 600 MHz and 150 MHz respectively. The spectral measurements are carried out at room temperature.

3. Computational details

In the present study, all the calculations are executed with the Gaussian 09W program [6]. By DFT calculations, the B3LYP functional combined with the 6-31+G(d, p) and 6-31++G(2d,2p) basis sets can be used to predict the geometrical parameters. The potential energy distributions (PEDs) are done with the help of MOLVIB program (Version V7.0-G77) written by Sundius [7, 8]. The vibrational frequency assignments are made with a high degree of confidence. In the present work, the scale factor of 0.9608 is used for B3LYP/6-31+G(d, p) level and 0.9026 for B3LYP/6-31++G(2d, 2p) level of theory. The ^1H and ^{13}C NMR chemical shifts are calculated with GIAO approach [9] by the applying B3LYP method. The natural bonding orbital (NBO) calculations [10] are performed using NBO 3.1 program as implemented in the Gaussian 09W package. The redistribution of electron density (ED) in various bonding and anti bonding orbital's along with $E_{(2)}$ energies have been calculated by natural bond orbital (NBO) using DFT method. The highest occupied molecular orbital (HOMO) energy, lowest unoccupied molecular orbital (LUMO) energy are calculated by B3LYP/6-31+G(d, p) basis set. The sites suitable for electrophilic and nucleophilic attacks have been determined by molecular electrostatic potential (MEP) surface and Fukui function analysis.

4. Results and Discussion

4.1 Potential Energy Surface scans and optimized geometrical parameters

Fig.1a shows the PES (Potential Energy Surface) scan energy profile of the NAA molecule, which was predicted as a function of dihedral angle C11-C14-O16-H17 rotation with respect to the relative energy. The dihedral angle was varied in steps of 10° , i.e., from 0° to 360° . The two minimum energy structures are obtained at the variation of the two torsion angles at 0° and 360° are identical because the hydroxyl group is acting oppositely but energetically both are equal. The energy values obtained from the scan output reveals that the structure having the dihedral angle C11-C14-O16-H17 at 0° possesses minimum energy. The optimized structural parameters (bond lengths, bond angles and dihedral angles) found by B3LYP/6-31+G(d, p) and B3LYP/6-31++G(2d, 2p) basis sets are presented in Table 1. The stable structure which produces the minimum energy of the molecule and crystal packing structure is shown in Figs. 1b and 1c, respectively.

4.2 Vibrational spectral analysis

The vibrational spectrum is mainly determined by the modes of the free molecules observed at higher wavenumbers

together with the lattice modes in the low wavenumbers region. The experimental and theoretical FT-IR and FT-Raman spectra are shown in Figs. 2 and 3. It should be noted that the calculations are made for a free

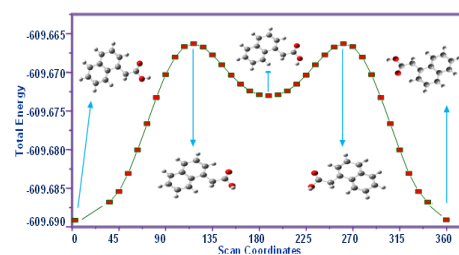


Fig 1a. Potential energy curve of Naphthalene-1-yl acetic acid along the C11-C14-O16-H17 dihedral angle calculated by B3LYP/6-31++G(2d, 2p) level of theory.

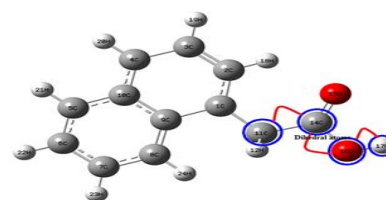


Fig1b. Stable structure for Naphthalene-1-yl acetic acid.

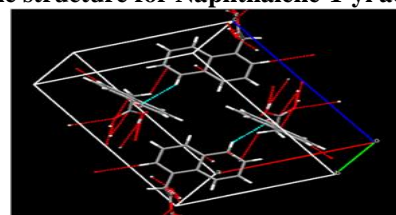


Fig1c. Crystal packing structure for Naphthalene-1-yl acetic acid.

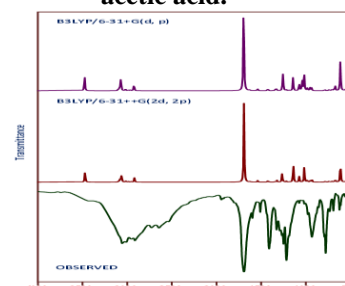


Fig 2. Observed and simulated infrared spectra of Naphthalene-1-yl acetic acid.

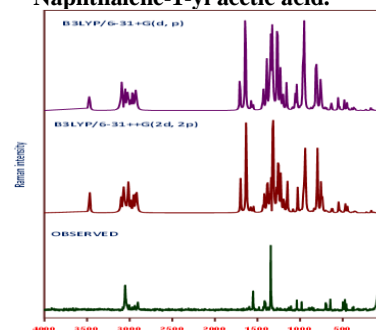


Fig 3. Observed and simulated Raman spectra of Naphthalene-1-yl acetic acid.

With the assumed structural models, the molecule belongs to C1 point group symmetry and has 24 atoms with 66 normal modes of vibrations. The observed (FT-IR and FT-Raman) wavenumbers and wavenumbers of vibrational modes calculated by B3LYP level using 6-31+G(d, p) and 6-31++G(2d, 2p) basis sets along with their PED of NAA are depicted in Table 2.

O-H vibrations

The OH group gives rise to three vibrations, stretching, in-plane bending and out-of-plane bending vibrations. The OH group vibrations are likely to be the most sensitive to the environment, so they show pronounced shifts in the spectra of the hydrogen-bonded species. In the case of un substituted naphthalene, it has been shown that the frequency of OH stretching vibration in the gas phase is 3500 cm^{-1} [11].

In the present case, a strong band in FT-IR spectrum at 3464 cm^{-1} is assigned to OH stretching vibration. s-strong, ms-medium strong, w-weak, vw-very weak, vs-very strong, n-stretching, ν_{ss} -sym. stretching, ν_{ass} -asym. stretching, δ -in-plane bending, γ -out-of-plane bending, ρ -scissoring, ω -wagging, σ -rocking, τ -twisting(out-of-plane bending)

C-H vibrations

The aromatic C-H stretching vibrations are normally found between $3100 - 3000\text{ cm}^{-1}$ [12-15].

Table 1: Optimized geometrical parameters of Naphthalen-1-ly acetic acid obtained B3LYP/ 6-31+G(d, p) and B3LYP/6-31++G(2d,2p) level of theory.

Bond lengths (Å)			Bond angles (degree)			Dihedral angles (degree)		
Parameters	6-31+G (d, p)	6-31++G (2d,2p)	Parameters	6-31+G (d, p)	6-31++G (2d,2p)	Parameters	6-31+G (d, p)	6-31++G (2d,2p)
C ₁ -C ₂	1.46	1.45	C ₂ -C ₁ -C ₉	120.07	120.08	C ₉ -C ₁ -C ₂ -C ₃	-2.75	-2.60
C ₁ -C ₉	1.43	1.43	C ₂ -C ₁ -C ₁₁	117.32	117.25	C ₉ -C ₁ -C ₂ -H ₁₈	177.31	177.46
C ₁ -C ₁₁	1.51	1.51	C ₉ -C ₁ -C ₁₁	122.61	122.67	C ₁₁ -C ₁ -C ₂ -C ₃	177.13	177.39
C ₂ -C ₃	1.36	1.36	C ₁ -C ₂ -C ₃	120.96	120.95	C ₁₁ -C ₁ -C ₂ -H ₁₈	-2.82	-2.55
C ₂ -H ₁₈	1.09	1.08	C ₁ -C ₂ -H ₁₈	118.25	118.26	C ₂ -C ₁ -C ₉ -C ₈	-176.81	-177.08
C ₃ -C ₄	1.44	1.44	C ₃ -C ₂ -H ₁₈	120.79	120.80	C ₂ -C ₁ -C ₉ -C ₁₀	3.35	3.08
C ₃ -H ₁₉	1.09	1.08	C ₂ -C ₃ -C ₄	119.94	119.92	C ₁₁ -C ₁ -C ₉ -C ₈	3.32	2.93
C ₄ -C ₁₀	1.42	1.41	C ₂ -C ₃ -H ₁₉	120.63	120.63	C ₁₁ -C ₁ -C ₉ -C ₁₀	-176.52	-176.92
C ₄ -H ₂₀	1.09	1.08	C ₄ -C ₃ -H ₁₉	119.43	119.45	C ₂ -C ₁ -C ₁₁ -H ₁₂	-152.35	-153.81
C ₅ -C ₆	1.43	1.43	C ₃ -C ₄ -C ₁₀	121.14	121.16	C ₂ -C ₁ -C ₁₁ -H ₁₃	-32.12	-33.31
C ₅ -C ₁₀	1.41	1.41	C ₃ -C ₄ -H ₂₀	119.76	119.77	C ₂ -C ₁ -C ₁₁ -C ₁₄	85.15	83.80
C ₅ -H ₂₁	1.09	1.08	C ₁₀ -C ₄ -H ₂₀	119.09	119.06	C ₉ -C ₁ -C ₁₁ -H ₁₂	27.52	26.18
C ₆ -C ₇	1.37	1.37	C ₆ -C ₅ -C ₁₀	121.68	121.68	C ₉ -C ₁ -C ₁₁ -H ₁₃	147.75	146.68
C ₆ -H ₂₂	1.09	1.08	C ₆ -C ₅ -H ₂₁	119.51	119.53	C ₉ -C ₁ -C ₁₁ -C ₁₄	-94.98	-96.20
C ₇ -C ₈	1.44	1.44	C ₁₀ -C ₅ -H ₂₁	118.81	118.80	C ₁ -C ₂ -C ₃ -C ₄	0.54	0.55
C ₇ -H ₂₃	1.09	1.08	C ₅ -C ₆ -C ₇	119.52	119.50	C ₁ -C ₂ -C ₃ -H ₁₉	-179.49	-179.47
C ₈ -C ₉	1.41	1.41	C ₅ -C ₆ -H ₂₂	119.48	119.50	H ₁₈ -C ₂ -C ₃ -C ₄	-179.52	-179.51
C ₈ -H ₂₄	1.08	1.08	C ₇ -C ₆ -H ₂₂	121.00	120.99	H ₁₈ -C ₂ -C ₃ -H ₁₉	0.45	0.47
C ₉ -C ₁₀	1.45	1.45	C ₆ -C ₇ -C ₈	120.08	120.07	C ₂ -C ₃ -C ₄ -C ₁₀	0.97	0.93
C ₁₁ -H ₁₂	1.09	1.09	C ₆ -C ₇ -H ₂₃	120.93	120.92	C ₂ -C ₃ -C ₄ -H ₂₀	-179.90	-179.91
C ₁₁ -H ₁₃	1.09	1.09	C ₈ -C ₇ -H ₂₃	118.99	119.01	H ₁₉ -C ₃ -C ₄ -C ₁₀	-179.00	-179.05
C ₁₁ -C ₁₄	1.52	1.52	C ₇ -C ₈ -C ₉	121.81	121.85	H ₁₉ -C ₃ -C ₄ -H ₂₀	0.13	0.11
C ₁₄ -O ₁₅	1.21	1.21	C ₇ -C ₈ -H ₂₄	118.19	118.15	C ₃ -C ₄ -C ₁₀ -C ₅	179.54	179.49
C ₁₄ -O ₁₆	1.36	1.35	C ₉ -C ₈ -H ₂₄	119.99	120.00	C ₃ -C ₄ -C ₁₀ -C ₉	-0.29	-0.38
O ₁₆ -H ₁₇	0.97	0.97	C ₁ -C ₉ -C ₈	123.68	123.70	H ₂₀ -C ₄ -C ₁₀ -C ₅	0.41	0.33
			C ₁ -C ₉ -C ₁₀	118.42	118.45	H ₂₀ -C ₄ -C ₁₀ -C ₉	-179.42	-179.55
			C ₈ -C ₉ -C ₁₀	117.89	117.85	C ₁₀ -C ₅ -C ₆ -C ₇	0.53	0.51
			C ₄ -C ₁₀ -C ₅	121.61	121.61	C ₁₀ -C ₅ -C ₆ -H ₂₂	-179.80	-179.82
			C ₄ -C ₁₀ -C ₉	119.39	119.36	H ₂₁ -C ₅ -C ₆ -C ₇	-179.49	-179.53
			C ₅ -C ₁₀ -C ₉	119.00	119.03	H ₂₁ -C ₅ -C ₆ -H ₂₂	0.19	0.14
			C ₁ -C ₁₁ -H ₁₂	111.66	111.72	C ₆ -C ₅ -C ₁₀ -C ₄	-179.35	-179.48
			C ₁ -C ₁₁ -H ₁₃	109.40	109.47	C ₆ -C ₅ -C ₁₀ -C ₉	0.47	0.39
			C ₁ -C ₁₁ -C ₁₄	111.16	110.86	H ₂₁ -C ₅ -C ₁₀ -C ₄	0.66	0.56
			H ₁₂ -C ₁₁ -H ₁₃	108.59	108.73	H ₂₁ -C ₅ -C ₁₀ -C ₉	-179.52	-179.57
			H ₁₂ -C ₁₁ -C ₁₄	109.41	109.46	C ₅ -C ₆ -C ₇ -C ₈	-0.41	-0.41
			H ₁₃ -C ₁₁ -C ₁₄	106.44	106.43	C ₅ -C ₆ -C ₇ -H ₂₃	179.37	179.43
			C ₁₁ -C ₁₄ -O ₁₅	125.28	125.19	H ₂₂ -C ₆ -C ₇ -C ₈	179.93	179.92
			C ₁₁ -C ₁₄ -O ₁₆	112.16	112.14	H ₂₂ -C ₆ -C ₇ -H ₂₃	-0.29	-0.24
			H ₁₅ -C ₁₄ -O ₁₆	122.54	122.65	C ₆ -C ₇ -C ₈ -C ₉	-0.74	-0.61
			C ₁₄ -O ₁₆ -H ₁₇	107.18	106.94	C ₆ -C ₇ -C ₈ -H ₂₄	178.04	178.35
						H ₂₃ -C ₇ -C ₈ -C ₉	179.48	179.55
						H ₂₃ -C ₇ -C ₈ -H ₂₄	-1.74	-1.50
						C ₇ -C ₈ -C ₉ -C ₁	-178.14	-178.36
						C ₇ -C ₈ -C ₉ -C ₁₀	1.71	1.48
						H ₂₄ -C ₈ -C ₉ -C ₁	3.11	2.70
						H ₂₄ -C ₈ -C ₉ -C ₁₀	-177.05	-177.46
						C ₁ -C ₉ -C ₁₀ -C ₄	-1.87	-1.62
						C ₁ -C ₉ -C ₁₀ -C ₅	178.30	178.50
						C ₈ -C ₉ -C ₁₀ -C ₄	178.28	178.52
						C ₈ -C ₉ -C ₁₀ -C ₅	-1.55	-1.35
						C ₁ -C ₁₁ -C ₁₄ -O ₁₅	-87.52	-88.10
						C ₁ -C ₁₁ -C ₁₄ -O ₁₆	91.00	90.34
						H ₁₂ -C ₁₁ -C ₁₄ -O ₁₅	148.70	148.20
						H ₁₂ -C ₁₁ -C ₁₄ -O ₁₆	-32.79	-33.35

Table 2. The calculated FT-IR and FT-Raman spectra of Naphthalene-1-yl acetic acid

S.No	Modes	Experimental Frequencies (cm ⁻¹)		Calculated frequencies (cm ⁻¹)				Vibrational Assignments/ PED (%)
		FT-IR	FT-Raman	B3LYP/ 6-31+G (d,p)	B3LYP/ 6-31++g (2d,2p)	B3LYP/ 6-31+G (d,p)	B3LYP/ 6-31++g (2d,2p)	
				Unscaled	Scaled	Unscaled	Scaled	
1	A'	3464w		3747	3470	3751	3465	vOH(98)
2	A'			3226	3096	3219	3088	vCH(98)
3	A'			3211	3079	3206	3074	vCH(99)
4	A'			3209	3066	3203	3061	vCH(98)
5	A'	3057s	3064vs	3196	3063	3190	3054	vCH(96)
6	A'	3012ms	3015w	3192	3018	3186	3011	vCH(99)
7	A'			3187	3013	3180	3007	vCH(97)
8	A'			3182	2983	3175	2980	vCH(98)
9	A'	2951vw	2952w	3126	2960	3121	2950	v _{ass} CH ₂ (92)
10	A'	2913s	2917s	3069	2920	3062	2914	v _{ss} CH ₂ (90)
11	A'	1692w	1646 w	1807	1696	1802	1691	vC=O(75), δ CC(12), δCO(10)
12	A'		1626ms	1654	1632	1647	1625	vCC(79), δCH(21)
13	A'	1568vs		1590	1565	1598	1568	vCC(78), δCH(21)
14	A'		1541w	1575	1542	1581	1540	δCH(86)
15	A'			1480	1431	1475	1428	ρCH ₂ (66), δCH(28)
16	A'	1411ms	1414w	1474	1419	1469	1411	δCH(79), vCC(12)
17	A'	1377vw	1377vs	1455	1382	1451	1375	δCH(78), vCC(10)
18	A'	1344vw		1432	1349	1429	1345	δCH(78), vCC(10)
19	A'	1327vw		1422	1335	1419	1326	δCH(78), vCC(12)
20	A'		1316w	1391	1320	1387	1315	vCC(69), δCH(21), σCH ₂ (10)
21	A'	1267ms		1358	1261	1360	1266	vOH(66), vCC(21), σCH ₂ (10)
22	A'	1249s	1246w	1336	1254	1336	1248	δCO(65), δOH(18), δCH(11)
23	A'	1217s		1308	1222	1304	1218	σCH ₂ (81), δCC(11)
24	A'	1185s		1275	1191	1273	1184	vCC(68), δOH(16)
25	A'		1143s	1229	1046	1232	1142	δCO(68), δCC(21),
26	A'		1120w	1210	1189	1206	1185	vCC(69), δCH(26)
27	A'	1074s	1074s	1197	1078	1195	1075	δCH(80)
28	A'	1041s		1183	1146	1182	1141	δCH(82)
29	A'		1019w	1138	1026	1136	1020	vCC(75), δCH(26)
30	A'	1017ms	1074s	1121	1022	1118	1018	τCH ₂ (69)
31	A'	977w	980w	1076	985	1072	984	vCC(69), σCH ₂ (11), δCH(10)
32	A'		952w	1043	957	1041	951	vCC(68), δRing(21)
33	A'	932w		993	940	989	932	vCC(68), δCC(21)
34	A'	857w		957	861	961	857	vCC(67), δCC(18)
35	A'		826w	954	830	957	825	γCH(80)

36	A'	792vs		927	799	925	790	vCC(75), δ CC(17), δ OH(10)
37	A'		784w	895	789	894	783	δ Ring (69)
38	A'		740mw	879	750	879	746	vCC(68), δ CO(21)
39	A'			849	744	852	741	γ CH(66)
40	A'	733w	728w	838	738	838	730	δ CO (71), δ CH(21)
41	A'			818	725	830	724	γ CH(66)
42	A'			802	712	801	710	δ Ring(72)
43	A'	691s	687s	782	692	786	689	γ CH(65)
44	A'	672w	672w	768	676	771	672	γ CH(66)
45	A'	623vs		729	627	745	625	γ CH(65)
46	A'		616w	708	620	710	617	vCH(69)
47	A'	612vw		697	615	702	612	vCH(71)
48	A'	538vs	541s	680	540	679	539	δ Ring(70)
49	A'		532w	627	538	627	530	δ Ring(71)
50	A'	518ms	517s	586	525	589	518	γ OH(61), γ Ring(20)
51	A'	502w	501ms	551	505	557	500	δ Ring(60)
52	A'		462w	530	466	530	462	δ CC(71), δ CH(23)
53	A'		434w	497	435	496	435	δ Ring(69)
54	A'		417s	486	420	489	416	γ Ring(54)
55	A'		378w	456	380	455	379	ψ CH ₂ (52), γ CC(27)
56	A'		350w	449	353	450	351	δ CC(53)
57	A'		336w	434	340	436	335	γ Ring(61)
58	A'			403	275	403	270	γ Ring(60)
59	A'		210w	325	213	327	210	γ Ring(58)
60	A'		154w	246	154	246	154	γ CO(56)
61	A'		126s	218	130	218	126	Butterfly(61)
62	A'			163	108	163	103	γ CC(55)
63	A'		69vs	131	70	132	68	γ CO(55)
64	A'			62	57	63	55	γ CC(49)
65	A'			51	25	50	23	γ Ring(51)
66	A'		14vw	34	16	34	14	γ Ring(50)

s-strong, ms-medium strong, w-weak, vw-very weak, vs-very strong, v-stretching, v_{ss}-sym. stretching, v_{ass}-asym. stretching, δ -in-plane bending, γ -out-of-plane bending, ρ -scissoring, ψ -wagging, σ -rocking, τ -twisting(out-of-plane bending)

The calculated wavenumbers in the range 3096-2983 cm^{-1} by B3LYP/6-31+G(d, p) method and 3088-2980 cm^{-1} by 6-31++G(d, p) method are assigned to C-H stretching vibrations. A strong and weak band appeared at 3064 and 3015 cm^{-1} in FT-Raman spectrum and at 3057 and 3012 cm^{-1} in the FT-IR spectrum are assigned to C-H stretching vibrations. As evident from the PED column, they are pure stretching vibrations almost contributing to above 96%. The C-H in-plane bending vibrations normally occur as a number of strong to weak intensity bands in the region 1300-1000 cm^{-1} [16]. In the present case, the C-H in-plane bending vibrations are computed in the range at 1419, 1382-1335 cm^{-1} by 6-31+G(d, p) method and 1411, 1375-1326 cm^{-1} by 6-31++G(2d, 2p) basis sets. The wavenumbers observed at 1411, 1377, 1344, 1327 cm^{-1} in FT-IR spectrum and 1414, 1377 cm^{-1} in FT-Raman spectrum show good agreement with predicted wavenumbers. Substitution pattern on the ring can be judged from the out-of-plane bending of the ring C-H bands, which are highly informative [17]. The C-H out-of-plane bending vibrations are normally observed in the region 1000-809 cm^{-1} [18-21]. The C-H out-of-plane bending vibrations are presented in Table 2.

C-C and C=O vibrations

The carbon-carbon stretching vibrations of the title compound were observed at 1568, 1411, 1344 and 1267 cm^{-1} in IR spectrum and the peaks observed at 1626, 1414 and 1377 cm^{-1} in Raman spectrum. The most characteristic features of the carboxylic group are single band observed usually in the region 1700-1600 cm^{-1} . This band is due to C=O stretching vibrations. In the present case, this mode appears at 1692 cm^{-1} in the IR spectrum and the FT-Raman value at 1646 cm^{-1} . The in-plane and out-of-plane bending vibrations of carbon-carbon groups are presented in Table 2. These assignments are in good agreement with the literature [22, 23].

Ring vibrations

Naphthalene ring vibrations are expected in the region 1620-1390 cm^{-1} . Naphthalene ring vibrations are found to make a major contribution in the IR and Raman spectra [24, 25]. The wavenumbers observed in FT-IR spectrum at 1568 cm^{-1} and in FT-Raman spectrum at 1626 cm^{-1} are assigned to ring vibrations. The scaled predicted harmonic wavenumbers at 1632 and 1565 cm^{-1} and other ring vibrations are shown a good agreement with the literature [24, 25]. These vibrations are mixed up with C-H in-plane bending vibrations and the PED corresponds to these vibrations are mixed modes as evident from Table 2.

4.3 NMR spectra

The gauge – including an atomic orbital (GIAO), ^{13}C NMR and ^1H NMR chemical shifts calculations of the title compound has been carried out by B3LYP functional with 6-31++G(2d, 2p) basis set. The GIAO approach to molecular systems was significantly improved by an efficient application of the method to the DFT calculation, using techniques borrowed from analytic derivative methodologies [26]. Relative chemical shifts were estimated using the corresponding TMS shielding calculated in advanced at the same theoretical level as the reference.

Experimental and theoretical chemical shifts of NAA in ^{13}C NMR and ^1H NMR was obtained and are presented in Table 3. The range of the ^{13}C NMR chemical shifts for a typical organic molecule usually is >100 ppm [27] and the accuracy ensures reliable interpretation of spectroscopic parameters. In the present study, the ^{13}C NMR chemical shifts

in the ring for NAA are >100 ppm, as they would be expected. The observed NMR spectra are shown in Fig. 4.

4.4 Mulliken and Natural charge analysis

The charge distribution on the molecule has an important influence on the vibrational spectra. Gaussian 09 offers several methods for the calculation of the atomic net charges. It has been long recognized that the total (net,) charge distribution in molecular ionic species is a very important parameter on the basis of which several important properties may be discussed. These include hydrogen bond proton acceptor ability [28], basicity, character (dipolar vs zwitterionic) of the studied species [29]. The comparison of Mulliken's net charges and the atomic natural ones is not an easy task since the theoretical background of the two methods is very different. The definition of Mulliken's charges is based on its population analysis. The Mulliken population analysis provides a partitioning of either the total charge density or an orbital density. The natural atomic charge is based on the theory of the natural population analysis. The analysis is carried out with natural bond orbitals (NBOs). The analysis is carried out with natural bond orbitals. The Mulliken's plot and their corresponding natural plots are shown in Fig.5 and the values are shown in Table 4.

The charge distribution of NAA (Table. 4) shows that all the hydrogen atoms and C1, C4, C5, C8 and C9 are positively charged; hence it is a donor atom, whereas the other carbon atoms are negative; hence it is an acceptor atom. The values of the natural atomic charges are different from Mulliken's atomic net charges. The tendency comparing the NAA natural atomic charges is very similar regarding both methods. The Mulliken charges of the atoms C5, C8 and C9 having a positive charge, while the natural charges become negative. It can be concluded that the natural atomic charges are more sensitive to the changes in the molecular structure than Mulliken's net charges.

4.5 NBO analysis

NBO analysis provides an efficient method for studying intra and intermolecular bonding and interactions among bonds and also provides a convenient basis for investigating charge transfer of conjugative interactions in molecular systems [30]. To investigate the intra and intermolecular interactions, the stabilization energies of the title compound is performed on NAA to elucidate intramolecular hydrogen bonding, intramolecular charge transfer (ICT) interactions and delocalization of π -electrons of the naphthalene ring.

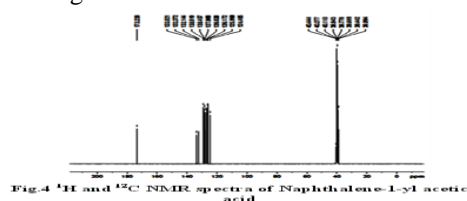


Fig. 4. ^1H and ^{13}C NMR spectra of Naphthalene-1-yl acetic acid.

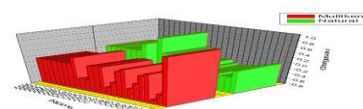


Fig. 5. Mulliken and Natural atomic charges for Naphthalene-1-yl acetic acid

Table 3.Theoretical and experimental ¹H NMR and ¹³C NMR spectra of Naphthalen-1-yl acetic acid (with respect to TMS, all values in ppm) for B3LYP/6-31++G(2d, 2p).

Atom Position	Experimental Method	B3LYP/6-31++G(2d, 2p)	Atom position	Experimental Method	B3LYP/6-31++G(2d, 2p)
C1	124.495	125.251	H12	38.994	39.192
C2	125.999	126.182	H13	39.442	40.158
C3	126.172	127.483	H17	39.609	40.565
C4	126.628	127.757	H18	39.776	40.710
C5	127.868	128.685	H19	39.943	40.895
C6	128.457	129.125	H20	40.110	41.230
C7	128.919	129.446	H21	40.277	41.325
C8	132.144	133.248	H22	40.444	41.549
C9	132.372	133.584			
C10	133.821	134.181			
C11	173.228	177.719			

Table 4. Mulliken and Natural atomic charges for Naphthalene-1-yl acetic acid at B3LYP/6-31++G(2d, 2p) basis set.

No	Atom	Mulliken charges (e)	Natural charges (e)	No	Atom	Mulliken charges (e)	Natural charges (e)
1	C ₁	0.908772	0.01993	13	H ₁₃	0.194223	0.27866
2	C ₂	-0.437710	-0.23753	14	C ₁₄	0.153507	0.81329
3	C ₃	-0.688090	-0.24157	15	O ₁₅	-0.404330	-0.60562
4	C ₄	0.220349	-0.18222	16	O ₁₆	-0.393510	-0.73050
5	C ₅	0.126130	-0.19193	17	H ₁₇	0.369839	0.52129
6	C ₆	-0.200770	-0.24385	18	H ₁₈	0.130931	0.25211
7	C ₇	-0.430120	-0.24619	19	H ₁₉	0.129808	0.24920
8	C ₈	0.241484	-0.19147	20	H ₂₀	0.126205	0.23644
9	C ₉	0.129183	-0.08086	21	H ₂₁	0.125235	0.23795
10	C ₁₀	-0.324760	-0.08445	22	H ₂₂	0.125613	0.24740
11	C ₁₁	-0.538810	-0.57898	23	H ₂₃	0.124408	0.24706
12	H ₁₂	0.191673	0.26957	24	H ₂₄	0.120739	0.24227

Table 5. Second order perturbation theory analysis of Fock matrix in NBO basis corresponding to inter molecular bands of Naphthalene-1-yl acetic acid.

S.No.	Donor NBO(i)	Acceptor NBO(j)	E(2) kJ/mol ⁻¹	E(j)-E(i) a.u	F(i,j) a.u
Unit-1					
1	LP(2) O15	σ*(C14-O16)	131.796	0.61	0.125
2	LP (2)O16	π*(C14-O15)	197.317	0.33	0.112
3	LP(3)O16	σ*(C11-C14)	19.372	0.88	0.064
Unit 2-1					
1	LP(1)H17	σ*(C14-O16)	40.125	0.19	0.071

F(i, j) is the Fock matrix elements between i and j NBO orbital's.

E(2) – mean energy of hyper conjugative interactions.

E(j) – E(i) – energy difference between donor and acceptor i and j NBO orbital's.

The change in the electron density (ED) in the (,) anti-bonding orbital's and E2 energies have been calculated by natural bond orbital (NBO) analysis [31] using the DFT methods to give clear evidence of stabilization originating from various molecular interactions. The hyper-conjugative interactions energy is deduced from the second-order perturbation approach [32].

$$E_2 = \Delta E_{ij} = q_i \frac{F(i,j)^2}{\epsilon_j - \epsilon_i}$$

where q_i is the donor orbital occupancy, and are diagonal elements and F(i,j) is the off diagonal NBO Fock matrix element. The larger E2 value, the more intensive is the interaction between electron donor to electron acceptors (i.e.,) the more donating tendency from electron donors to electron acceptors and the greater the extent of conjugation of the whole system. In the present analysis, the strong intramolecular hyper-conjugation interaction of and electrons of C-C to C-C anti-bonds in the ring leads to stabilization of the ring.

The NBO analysis also describes the bonding in terms of the natural hybrid orbital C8-H24, which occupancy a higher energy orbital (1.98981 a.u) with considerable p-character (72.71%). The hyper-conjugative interaction of (lone pair) LP (O16) of *(C14-O15) which increased ED that weakens the respective bonds leading to stabilization of 197.3174 kJ/mol-1. These results are tabulated in Tables 5 and 6.

4.6 Non-linear optical activity

Nonlinear optics deals with the interaction of applied electromagnetic fields in various materials to generate new electromagnetic fields, altered in wavenumber, phase, or other physical properties [33]. The calculated first hyper-polarizability of the title compound is 5.19728×10⁻³⁰ esu which is more than that of standard NLO material urea (0.13 × 10⁻³⁰ esu) [34]. The mean hyper-polarizability of NAA was reported as 1.1348×10⁻³⁰ esu and a title compound is an attractive object for future studies of nonlinear optical properties. The average second hyper-polarizability has been calculated by using the following expression.

$$\gamma_{av} = 1/5[\gamma_{xxxx} + \gamma_{yyyy} + \gamma_{zzzz} + 2\gamma_{xxyy} + 2\gamma_{xxzz} + 2\gamma_{yyzz}]$$

The amount of charge transfer for the molecule depends on the nature of the end group of the molecule. The increase of - conjugated chain length in organic molecules, in general, enhances the magnitude of hyperpolarizability. The calculated value of γ_{av} for the title compound is 1.0679×10^{-36} esu. The larger component of second hyper-polarizability is associated with the larger ground state polarization which leads to strong electronic coupling between the ground and the low lying excited state. Thus the present investigation provides a new route to design high-performance NLO materials. First order hyper-polarizability, mean polarizability, dipole moment and second order hyper-polarizability values are shown in Table 7.

4.7 HOMO – LUMO analysis

The HOMO – LUMO energy of NAA by DFT B3LYP/6-31++G(2d, 2p) basis set was calculated. The highest occupied molecular orbital (HOMO) and lowest unoccupied molecular orbital (LUMO) is the main orbital take part in chemical stability. The HOMO represents the ability to donate an electron, LUMO as an electron acceptor represents the

ability to obtain an electron. For NAA the highest occupied molecular orbital HOMO lying at -6.1822 eV is a delocalized orbital. The HOMO-1, lying -6.9435 eV below the HOMO, is a delocalized orbital over the entire molecules. While the HOMO-2 lying -7.9215 eV below the HOMO respectively are orbital that localized in benzene ring whereas the LUMO lying at -1.4634 eV. That is localized orbital the LUMO+1, lying about -0.7796 eV below LUMO, is also an orbital. The HOMO, LUMO energy gap plots are shown in Fig. 6.

The most important application of the DOS (Fig.7) plots is to demonstrate molecule orbital (MO) compositions and their contributions to chemical bonding through the PDOS plots which are also referred in the literature as Crystal Orbital Overlap Population (COOP) diagrams. The COOP (or PDOS) is similar to DOS because it results from multiplying DOS by the overlap population. The PDOS shows the bonding anti-bonding and non-bonding interaction of the two orbitals, atoms or groups.

Table 6. NBO results showing the formation of Lewis and non-Lewis orbitals of Naphthalene-1-yl acetic acid.

Bond orbital	Occupancies (e)	EDA %	EDB %	Polarization coefficient of bond orbital		Hybrid	S (%)	P (%)
				I Atom	II atom			
C ₁ -C ₂	1.97597	51.15	48.85	0.7152	0.6989	SP ^{1.75}	36.32	63.65
						SP ^{1.87}	34.83	65.13
C ₁ -C ₉	1.97130	49.54	50.46	0.7039	0.7103	SP ^{1.92}	34.28	65.68
						SP ^{1.98}	33.53	66.44
C ₁ -C ₁₁	1.96589	49.27	50.73	0.7019	0.7123	SP ^{2.40}	29.37	70.60
						SP ^{2.86}	25.90	74.06
C ₂ -C ₃	1.97744	50.39	49.61	0.7099	0.7043	SP ^{1.92}	34.19	65.77
						SP ^{1.94}	33.96	66.00
C ₂ -H ₁₈	1.97905	62.95	37.05	0.7934	0.6087	SP ^{2.23}	30.94	69.02
						SP ^{0.00}	99.94	0.06
C ₃ -C ₄	1.98133	49.82	50.18	0.7058	0.7084	SP ^{1.81}	35.60	64.35
						SP ^{1.78}	35.94	64.02
C ₃ -H ₁₉	1.98247	62.39	37.61	0.7899	0.6132	SP ^{2.29}	30.39	69.57
						SP ^{0.00}	99.95	0.05
C ₄ -C ₁₀	1.97577	48.41	51.59	0.6958	0.6958	SP ^{1.97}	33.68	66.27
						SP ^{1.97}	33.63	66.33
C ₄ -H ₂₀	1.98131	62.17	37.83	0.7885	0.6150	SP ^{2.30}	30.33	69.63
						SP ^{0.00}	99.95	0.05
C ₅ -C ₆	1.98135	50.19	49.81	0.7084	0.7058	SP ^{1.79}	35.86	64.10
						SP ^{1.80}	35.64	64.32
C ₅ -C ₁₀	1.97595	48.51	51.49	0.6965	0.7176	SP ^{1.97}	33.71	66.25
						SP ^{1.97}	33.69	66.28
C ₅ -H ₂₁	1.98108	62.22	37.78	0.7888	0.6146	SP ^{2.29}	30.39	69.57
						SP ^{0.00}	99.95	0.05
C ₆ -C ₇	1.97978	49.97	50.03	0.7069	0.7073	SP ^{1.94}	34.03	65.93
						SP ^{1.94}	34.04	65.92
C ₆ -H ₂₂	1.98246	62.34	37.66	0.7896	0.6137	SP ^{2.30}	30.28	69.68
						SP ^{0.00}	99.95	0.05
C ₇ -C ₈	1.98119	49.66	50.34	0.7047	0.7095	SP ^{1.80}	35.66	64.30
						SP ^{1.76}	36.18	63.78
C ₇ -H ₂₃	1.98247	62.33	37.67	0.7895	0.6138	SP ^{2.30}	30.27	69.69
						SP ^{0.00}	99.95	0.05
C ₈ -H ₂₄	1.97986	61.96	38.04	0.7872	0.6168	SP ^{2.29}	30.41	69.55
						SP ^{0.00}	99.95	0.05
C ₉ -C ₁₀	1.96540	50.32	49.68	0.7094	0.7048	SP ^{2.02}	33.09	66.87
						SP ^{2.07}	32.61	67.35
C ₁₁ -H ₁₂	1.97322	63.80	36.20	0.7987	0.6017	SP ^{2.88}	25.79	74.16
						SP ^{0.00}	99.95	0.05
C ₁₁ -C ₁₃	1.96463	63.82	36.18	0.7989	0.6015	SP ^{2.95}	25.28	74.68
						SP ^{0.00}	99.95	0.05
C ₁₁ -C ₁₄	1.97717	50.50	49.50	0.7106	0.7036	SP ^{3.34}	23.01	76.93
						SP ^{1.55}	39.18	60.76
C ₁₄ -O ₁₅	1.99738	34.64	65.36	0.5886	0.8085	SP ^{1.95}	33.90	65.99
						SP ^{1.54}	39.27	60.32
C ₁₄ -O ₁₆	1.98981	31.12	68.88	0.5578	0.8300	SP ^{2.69}	27.01	72.71
						SP ^{2.66}	27.28	72.64

A positive value of the COOP indicates a bonding interaction, whereas a negative value means an anti-bonding interaction and zero value indicated non-bonding interactions [35]. The PDOS mainly presents the composition of the fragment orbitals as seen from Fig. 8. PDOS mainly presents the composition of fragment orbitals contributing to molecular orbitals. $\alpha\beta$ DOS shows the bonding, sum of a positive and negative electron with nature of the interaction of two orbitals, atoms or groups. In NAA there exist 50α and β -electrons, totally 4 electrons are occupied in DOS both the HOMO and LUMO are the main orbital taking part in the chemical reaction. The energy gap between the HOMO and LUMO is a critical parameter in determining molecular electrical transport properties because it is a measure of electron conductivity [36]. A positive value of $\alpha\beta$ DOS indicates a bonding interaction, a negative value means that there is an anti-bonding interaction and zero value indicates nonbonding interactions. The DOS in terms of Mulliken population analysis was calculated using Gausssum program. The results provide a pictorial representation of MOs. The PDOS and TDOS (Figs. 8 and 9) diagram may enable to ascertain the orbital composition characteristics with respect to the particular fragments.

4.8 Molecular electrostatic potential surface analysis

The molecular electrostatic potential (MEP) surface is a well-established approach for the determination of reactive behavior of a molecule toward electrophiles. In order to find the reactive behavior of the molecule, the atomic charge calculation scheme has been used in which the atomic charges are fitted to reproduce the MEP at a number of points around the molecule [37-39]. The calculated electrostatic point charges and electrostatic potential $V(\cdot)$ on individual atoms due to the charge distribution are given in Table 10 and the generated MEP surface for all the conformers of NAA are given in Fig. 10. The red color surface surrounded by the oxygen atoms represents the region of maximum electro negativity and blue color surface accumulated on the hydrogen atoms shows their electro positivity. The different values of the electrostatic potential at the MEP surface are represented by different colors: red, blue and green represent the regions of most negative, most positive and zero electrostatic potential, respectively.

Table 7. Electric dipole moment μ (debye), mean polarizability α (e.s.u.), anisotropy polarizability $\Delta\alpha$ (e.s.u.), first order hyperpolarizability $\beta_{tot}(\times 10^{-30}$ e.s.u.) and $\gamma_{av}(\times 10^{-36}$ e.s.u.) for Naphthalene-1-yl acetic acid at B3LYP/ 6-31+G(d, p) method.

Parameters	B3LYP	Parameters	B3LYP
	6-31++G(2d, 2p)		6-31++G(2d, 2p)
μ_x	-0.7256	β_{xxx}	37.5467
μ_y	-0.7235	β_{yyy}	2.3678
μ_z	1.2063	β_{zzz}	1.3235
μ	1.5828	β_{xvy}	1.6899
α_{xx}	-75.4250	β_{xxv}	-3.7450
α_{xy}	-3.5786	β_{xxz}	32.2144
α_{xz}	6.0209	β_{xzz}	11.4766
α_{yy}	-74.6141	β_{vzz}	-3.0969
α_{vz}	2.7004	β_{vzv}	-1.4832
α_{zz}	-88.7275	β_{xvz}	5.7764
A	-79.5889	β_{tot}	5.19728×10^{-30}
$\Delta\alpha$	1.1348×10^{-30}	γ_{xxxx}	-2497.0240
γ_{vvvv}	-903.3784	$2\gamma_{xxzz}$	-624.8302
γ_{zzzz}	-184.1739	$2\gamma_{vvzz}$	-211.7690
$2\gamma_{xxvy}$	-561.1309	γ_{av}	1.0679×10^{-36}

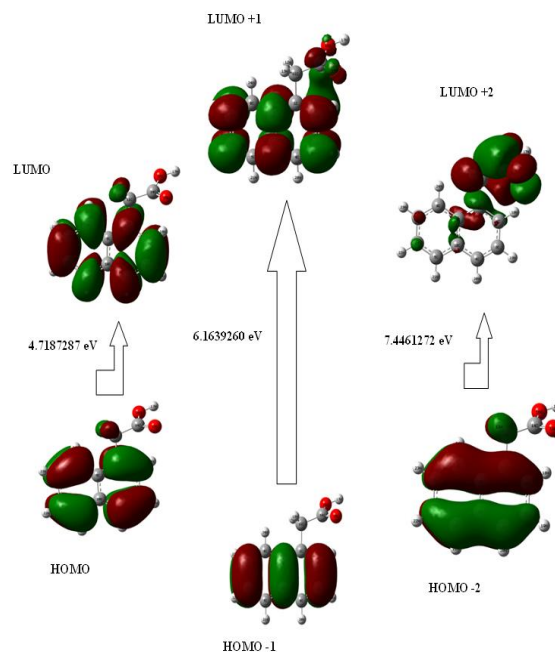


Fig 6. Atomic orbital HOMO and LUMO composition of the frontier molecular orbital for Naphthalene-1-yl acetic acid.

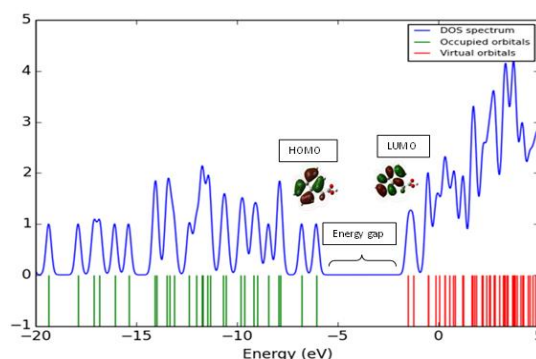


Fig 7. DOS spectrum for Naphthalene-1-yl acetic acid.

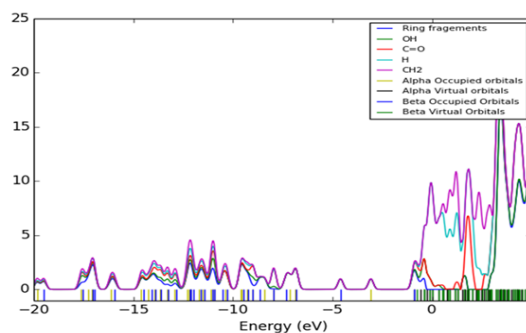


Fig 8. PDOS spectrum for Naphthalene-1-yl acetic acid.

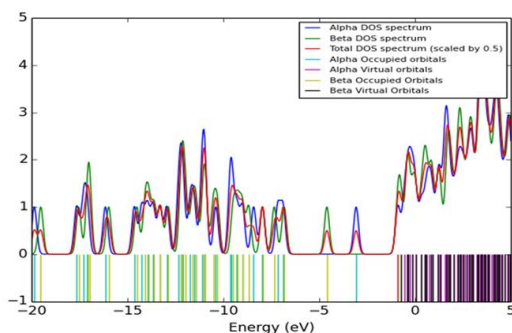


Fig 9. TDOS spectrum for Naphthalene-1-yl acetic acid.

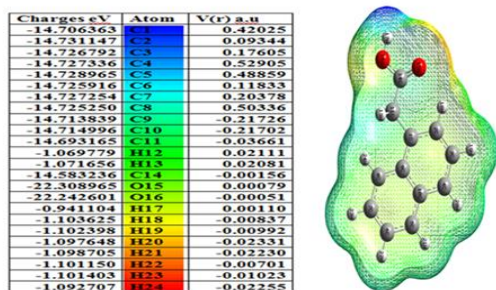


Fig10. Molecular electrostatic potential map for Naphthalene-1-yl acetic acid.

The negative electrostatic potential corresponds to an attraction of the proton by the aggregate electron density in the molecule (shades of red), while the positive electrostatic potential corresponds to the repulsion of the positive (Blue) regions to nucleophilic reactivity (Fig. 10). From the MEP it is evident that the negative charge covers the C=O group and the positive region is over the rings.

4.9 Local and global reactivity descriptors

Although the MEP surface analysis is a good indicator of electrophilic and nucleophilic sites, it has some limitations analyzing nucleophiles. Because the $V(r)$ for any free neutral atom is positive everywhere and it is maximum at the nucleus [40-42]. When atoms combine to form a molecule, the accompanying rearrangement of electrons produces one or more regions negative electrostatic potential and other regions of atoms have positive electrostatic potential. On the other hand, the positive regions do not have maxima other than at the positions of the nuclei. Thus, $V(r)$ provides clear-cut guidelines to the sites, which are most attractive to the nucleophiles [43]. These barriers can be resolved by Fukui function analysis.

Since the Fukui functions result from the Hirshfeld partitioning of the electron density of neutral atom (N) along with that of anionic (N+1) and cationic (N-1) species, it provides more precise site selectivity and qualitative reactivity descriptors within the molecule. The condensed forms of Fukui functions such as, respectively for the radical, nucleophilic and electrophilic attack in an atom A of a molecule can be expressed as [44],

$$f_A^+(\vec{r}) = q_{A(N)} - q_{A(N+1)}$$

$$f_A^-(\vec{r}) = q_{A(N-1)} - q_{A(N)}$$

$$f_A^0(\vec{r}) = \frac{1}{2} [q_{A(N-1)} - q_{A(N+1)}]$$

The calculated Fukui functions along with relative electrophilicity and nucleophilicity indices are depicted in Table 9. In the present work, the local softness (s_A^+ and s_A^-) and the electrophilicity (w_A^+ and w_A^-) indices for the aforesaid sites are also calculated as follows,

$$s_A^+ = s_A^{f^+}, s_A^- = s_A^{f^-}$$

$$w_A^+ = f_A^+, w_A^- = f_A^-$$

where s and w are represented global softness and electrophilicity indices of atoms in a molecule. As both the local softness and electrophilicity are expressed in terms of their corresponding Fukui indices, they yield respective proportionate values. However, s and w values, it can be estimated the tendency of an atomic center to behave either like an electrophile or nucleophile. As an individual and values are basis set and correlation effect dependent, the redistribution of electron densities with the change in a

number of electrons is not clearly known [45]. Table 8 denotes the value of electrophilicity and nucleophilicity. Hence, the relative electrophilicity and relative nucleophilicity are calculated in the present study. The site having the highest is the most probable site to be attacked by a nucleophile, and the site having the highest ratio is the most probable site to be attacked by an electrophile. The global reactivity descriptors such as energy band gap, ionization potential (I), electron affinity (A), electronegativity (χ), chemical potential (μ), global hardness (η), global softness (S), and global electrophilicity index (ω) are required to understand the biological activity of a molecule. These values are tabulated in Table 9. Using Koopman's theorem for closed-shell molecules, the above factors are defined as suggested by Parthasarathi et al [47].

4.10 Hirshfeld Surface analysis

Hirshfeld surfaces facilitate a novel method of visualizing intermolecular interactions by colour-coding short or long contact and the colour intensity indicates the relative strength of the interactions. Additionally, the size and shape of a Hirshfeld surface also reflect the interplay between different atoms and intermolecular contacts in a crystal. The 2-D fingerprint plots, which are derived from the Hirshfeld surfaces, complement these. They quantitatively summarize the nature and type of intermolecular contacts experienced by the molecules in the crystal. Each point on the standard 2-D graph represents a bin formed by discrete intervals of d_e and d_i and the points on the surfaces are colored as a function of the fraction of the surface points in the bin [46]. For instance, the blue color indicates relatively few points while the green color means moderate points and the red color suggests many points. The 2-D fingerprint plots can also be broken down to give the relative contribution to the Hirshfeld surface area of each type of interaction present, quoted as the "contact contribution". For a given crystal structure, the Hirshfeld surfaces, as well as fingerprint plots, are all unique [47] and the number of unique Hirshfeld surfaces depends on the number of crystallographically independent molecules in the corresponding asymmetric unit [48].

Because of the limitation of d_e and d_i when taking into account the relative sizes of the atoms, the normalized contact distance d_{norm} based on d_e , d_i and r_{vdW} (the van der Waals (vdW)) radius of the atom is usually employed for the analysis [49]. The value of d_{norm} is negative or positive when the intermolecular contacts are shorter or longer than r_{vdW} , respectively.

The d_{norm} Hirshfeld surfaces are displayed using a red-white-blue colour scheme, where red highlights shorter contacts, white is used for contacts around the r_{vdW} , separation and blue is for longer contacts. In addition, due to the symmetry between d_e and d_i in the expression for d_{norm} , both the points where two Hirshfeld surfaces touch will be marked with a red spot identical in color intensity as well as in size and shape [50].

$$d_{norm} = \frac{d_i - r_{vdW}}{r_i^{vdW}} + \frac{d_e - r_{vdW}}{r_e^{vdW}}$$

The molecular graphics were prepared by using the DIAMOND [51] and Mercury programs [52]. This CIF data can be obtained free of charge from the chemspider data via www.chemspider.com/cif. The Hirshfeld surfaces of the NAA molecule is illustrated in Fig.11 which shows surfaces that have been mapped over d_{norm} (-0.705 to 1.471Å). It is clear that the information present in Table 10 is summarized effectively in these spots, with the large circular depressions visible on the surfaces indicative of strong H...H interactions

and the other color points in the two-dimensional fingerprint plots are indicative of short contacts for the O...O, C...C and O...O interactions. In the case of the molecule, the H-H intermolecular interactions appear as a sharp small spike in the two-dimensional fingerprint plots with $d_i = 1.992 \text{ \AA}$ and $d_e = 1.956 \text{ \AA}$. The H...H interactions have a more significant contribution to the total Hirshfeld surfaces of a molecule comprising 43.4 % and reflected in the middle of the scattered points in the two-dimensional fingerprint plot. The H...O interactions comprise 21.9 % to the total Hirshfeld surfaces and appear as a narrow large blunt spike in the fingerprint plot. The C...C interactions also have a relatively significant contribution to the total Hirshfeld surfaces of the molecule, which comprises 1.0 % as indicated by the small spike in the middle of the 2-D fingerprint plot. There also exist lone-pair oxygen atoms interactions comprising 0.5 % of the total Hirshfeld surfaces. C...O interaction comprises 0.4 %. These interactions are around the rvdW separation.

Apart from those mentioned above, the presence of C...H interactions percentage is observed in Fig. 11, its contributing 32.8 % to the total Hirshfeld surfaces, an are indicated by the "wings" in the upper left and lower right of the 2D fingerprint plot. The H...H interactions are still the main contribution to the total Hirshfeld surfaces 43.5 % and can be viewed as the "ridge" of the 2-D fingerprint plots. The C...H interactions contribute 32.8 % to the total Hirshfeld surfaces and are also characterized by "wings" in the upper left and lower right regions of the 2-D fingerprint plots.

4.11 Molecular docking studies

The prediction of molecular interactions between the lead molecule and targets (proteins, enzymes; etc.) of biological interest has become of great importance in the field of drug discovery. In addition, by docking analysis of the lead molecule with several protein targets, one can easily find insights into the underlying molecular mechanisms of selectivity [53]. These proteins were selected on the basis of the probability of binding given by the Swiss target prediction web interface [54]. Molecular docking study was performed

on Auto Dock Tool software [55]. The 3D crystal structure of the protein was taken from Protein Data Bank (PDB ID: 2P1O, 3N8I, 4O1Y and 1WOX) [56-57]. Docking protein was prepared, firstly the B and C and other chain were removed and then the receptor was prepared by the cleaning of all heteroatom's (i.e., non-receptor atoms such as water, ions, co-crystallized ligand, etc.). After that Geistenger charges and polar hydrogens were assigned and receptor input file was prepared in PDBQT format for Auto-Dock-Tool by using the Auto-Dock Tools package. Ligand input file was also arranged in PDBQT format tool. The docking area was defined around the ATP binding site, which was determined in the crystal structure, by a grid box of $126\text{\AA} \times 126\text{\AA}$ using 0.375\AA grid point spacing in Auto-Grid. The docking conformations of ligands in the binding sites of the receptor were searched with Lamarckian genetic Algorithm (LGA) in Autodock. Finally, the co-crystal inhibitor ligand of the receptor was docked again for the confirmation of the docking protocol. Discovery Studio Visualizer was used for analyzing the detailed interactions. NAA was prepared for docking by minimizing its energy at B3LYP/6-31++G(2d, 2p) level of theory.

Table 10. Summary of the various contact contributions to the Naphthalen-1-yl acetic acid of Hirshfeld surface.

Name of the Interactions	Percentage of Interactions
C...C	1.0 %
C...H/H...C	32.6 %
C...O/O...C	0.4 %
H...H	43.4 %
H...O/O...H	21.9 %
O...O	0.5 %

After then the title compound was docked with the same protocol as given above and binding properties determined with Autodock. The binding affinity (-8.18 kcal/mol) and RMSD 25.24 Å values of the title compound were found reliable (Table 11).

Table 8. Fukui functions (f_A^+ , f_A^- , f_A^0), relative electrophilicity (f_A^+/f_A^-) and nucleophilicity (f_A^-/f_A^+) indices of Naphthalene-1-yl acetic acid by DFT-D/B3LYP/6-31++G(2d, 2p) method.

S. No	Atoms	qN	qN-1	qN-1	f_A^+	f_A^-	f_A^0	f_A^+/f_A^-	f_A^-/f_A^+
1	C1	-0.0167	-0.0438	0.0666	-0.0552	-0.0833	-0.0271	3.0740	0.3253
2	C2	-0.0645	-0.1168	0.0229	-0.0699	-0.0874	-0.0523	1.6712	0.5984
3	C3	-0.0125	-0.1026	0.0914	-0.0970	-0.1040	-0.0901	1.1541	0.8665
4	C4	-0.0069	-0.0950	0.1274	-0.1112	-0.1342	-0.0882	1.5227	0.6567
5	C5	0.0043	-0.0912	0.1184	-0.1048	-0.1141	-0.0955	1.1950	0.8368
6	C6	-0.0051	-0.0832	0.1018	-0.0925	-0.1069	-0.0781	1.3686	0.7307
7	C7	-0.0024	-0.0994	0.0976	-0.0985	-0.1000	-0.0970	1.0314	0.9695
8	C8	-0.0080	-0.0896	0.1036	-0.0966	-0.1116	-0.0816	1.3687	0.7306
9	C9	-0.0083	-0.0182	0.0043	-0.0113	-0.0126	-0.0099	1.2697	0.7876
10	C10	-0.0034	-0.0196	0.0107	-0.0151	-0.0141	-0.0162	0.8706	1.1486
11	C11	0.0787	-0.0425	0.1348	-0.0886	-0.0561	-0.1212	0.4631	2.1594
12	C14	0.2457	0.1653	0.2489	-0.0418	-0.0032	-0.0804	0.0399	25.0874
13	O15	-0.2825	-0.3797	-0.2371	-0.0713	-0.0454	-0.0973	0.4669	2.1420
14	O16	0.0813	0.0166	0.1084	-0.0459	-0.0271	-0.0646	0.4190	2.3865

Table 9. HOMO and LUMO energies gap values (eV) and related molecular properties of Naphthalene -1- ly acetic acid based on B3LYP/6-31++G(2d, 2p) method.

Molecular properties	Energy (eV)	Energy gap (eV)	Ionization potential (I) (eV)	Electron affinity (A) (eV)	Global hardness (η)	Electro negativit y (χ) (eV)	Chemical softness (σ) (eV)	Chemical Potential (μ) (eV)	Global Electrophilicity (ω) (eV)
E_{HOMO}	-6.1822	4.7187	6.1822	1.4634	7.6456	3.8228	0.1308	-3.8228	0.9557
E_{LUMO}	-1.4634								
$E_{\text{HOMO-1}}$	-6.9435	6.1639	6.9435	0.7796	7.7231	3.8616	0.1295	-3.8616	1.0310
$E_{\text{LUMO+1}}$	-0.7796								
$E_{\text{HOMO-2}}$	-7.9215	7.4461	7.9215	0.4754	8.3969	4.1984	0.1191	-4.1984	1.0496
$E_{\text{LUMO+2}}$	-0.4754								

Table 11. Binding energy values of different poses of the Naphthalene-1-yl acetic acid predicted by Autodock Tool.

Protein PDB ID	Bonded residues	No. of Hydrogen bond	Bond Distance Å	Estimated inhibition Constant (μM)	Binding energy (kcal/mol)	Reference RMSD Å
2P1O	LYS 92 MET 91	2	2.6 1.9	86.55	-5.54	168.17
3N8I	GLN 105 ARG 101 ARG 101 LYS 102	4	2.0 1.9 1.9 1.9	1.0	-8.18	25.24
4O1Y	ARG 6	1	1.9	21.83	-6.36	41.16
1WOX	SER 132 LYS 171 ARG 175	3	1.7 2.2 2.8	10.29	-6.80	18.92

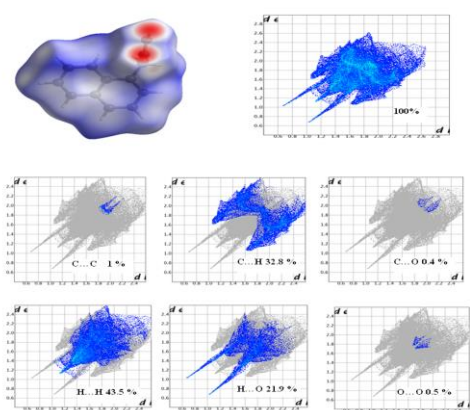


Fig 11. Hirshfeld surface fingerprint plots of the nearest internal distance (d_i) vs the nearest external distance (d_e) for each of the crystallographically independent molecule in the Naphthalene-1-yl acetic acid. Each point on an HS can be represented by a coordinate (d_i , d_e). The colors represent the number of points with a given fingerprint plot coordinate (hot colors represent many points, cool colors represent few points).

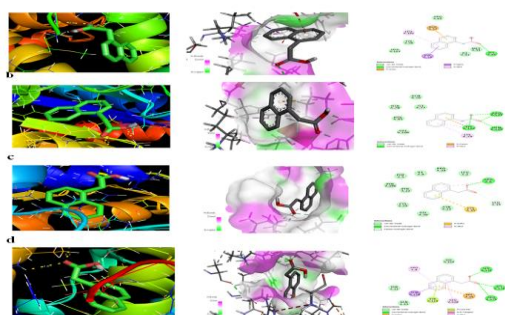


Fig. 12 NAA interaction of protein (a. 2P1O, b. 3N8I, c. 4O1Y, d. 1WOX) The docked protocol reproduced the co-crystallized conformation with H-bond (green), π -alkyl (pink), π - π (magenta) and H-bond receptor surface shown.

There are some close contacts such as Vander Walls interactions with the 2P1O, 3N8I, 4O1Y and 1WOX bases of protein. Also, there is alkyl interaction commonly present four proteins between naphthalene ring of ligand and the residues as seen in Fig.12. The confirmation of interaction profile of the title compound was provided by this way. There are four best hydrogen bonds with these residues GLN 105, ARG 101, ARG 101 and LYS102 base which was same like docking

results. Lastly, there are VanderWalls interactions between the ligand and residues in Fig 12

5. Conclusion

FT-IR and FT-Raman spectra of NAA were studied experimentally and theoretically. The molecular geometry and wavenumbers were calculated using DFT/B3LYP/6-31+G(d, p) and 6-31++G(2d, 2p). The lowering of the HOMO – LUMO energy gap value has a substantial influence on the intramolecular charge transfer and bioactivity of the molecule. A detailed molecular picture of the title compound and its interactions were obtained from NBO analysis. As MEP map give the details, the negative electrostatic potential regions are mainly contributed to the carbonyl group and are possible sites for electrophilic attack and the positive regions are contributed in aromatic rings, indicating possible sites for nucleophilic attack. Hirshfeld surface and fingerprint plot analysis provide rapid quantitative insight into the intermolecular interactions in complex molecular solids. The higher interactions appear in H...H, C...H/H...C contacts, and these relatively weak interactions have clear signatures in the fingerprint plots. From the molecular docking results, we suggest that the title compound might exhibit inhibitory activity against 2P1O, 3N8I, 4O1Y, 1WOX and may act as muscle blind agent.

REFERENCES

- [1] F. Warnia, D. Mackay, Peer Reviewed: Tracking the Distribution of Persistent Organic Pollutants Control strategies for these contaminants will require a better understanding of how they move around the globe Environ. Sci. Technol. A 30 (1996) 390–396.
- [2] H. Morikawa, M. Takahashi, Cultured cells of Australian laurel, Pittosporaceae and a method for culturing tissues by using said cultured cells, (2004) 10-15.
- [3] C.D.S. Tomlin, The Pesticide Manual, 14th ed. UK, 2006.
- [4] A. Navalón, R. Blanc, J.L. Vilchez, Determination of 1-naphthylacetic acid in commercial formulations and natural waters by solid-phase spectrofluorimetry Microchim. Acta, 126 (1997) 33–38.
- [5] Naduvilpurakkal, B. Shibin, Radhakrishnan Sreekanth, Usha, K. Aravind, M. Kadavilpparampu, Afsal Mohammed, V. Narayana, Chandrashekhar, Jayan Joseph, K. Sisir, Sarkar, B. Devidas, T. Naik, Charuvila, Aravindakumar, Radical chemistry of glucosamine naphthalene acetic acid and naphthalene acetic acid: a pulse radiolysis study J. Phys. Org. Chem. 27 (2014) 478-483.

- [6] M.J. Frisch, G.W. Trucks, H.B. Schkegel, G.C. Scuseria, M.A. Robb, J.R. Cheeseman, G. Scalmani, V. Barone, B. Mennucci, G.A. Bloino, G. Zheng, J.L. Sonnenberg, M. Hada, M. Ehara, K. Toyota, R. Fukuda, J. Hasegawa, M. Ishida, T. Nakajima, Y. Honda, O. Kitao, H. Nakai, T. Vreven, J.A. Montgomery, J.E. Peralta, F. Ogliaro, M. Bearpark, J.J. Heyd, E. Brothers, K.N. Kudin, V.N. Staroverov, T. Keith, R. Kobayashi, J. Normand, K. Raghavachari, A. Rendell, J.C. Burant, S.S. Iyengar, J. Tomasi, M. Cossi, N. Rega, J.M. Millam, M. Klene, J.E. Knox, J.B. Cross, V. Bakken, C. Adamo, J. Jaramillo, R. Gomperts, R.E. Stratmann, O. Yazyev, A.J. Austin, R. Cammi, C. Pomelli, J.W. Ochterski, R.L. Martin, K. Morokuma, V.G. Zakrzewski, G.A. Voth, P. Salvador, J.J. Dannenberg, S. Dapprich, A.D. Daniels, O. Farkas, J.B. Foresman, J.V. Ortiz, J. Cioslowski, D.J. Fox, Gaussian Inc, Wallingford CT, Gaussian 09, Revision D.01, 2013.
- [7] T. Sundius, Scaling of ab initio force fields by MOLVIB, *Vib. Spectrosc.* 29 (2002) 89–95.
- [8] MOLVIB (V.7.0): Calculation of Harmonic Force Fields and Vibrational Modes of Molecules, QCPE Program No. 807, 2002.
- [9] R. Ditchfield, Molecular Orbital Theory of Magnetic Shielding and Magnetic Susceptibility, *J. Chem. Phys.* 56 (1972) 5688–5691.
- [10] K. Wolinski, J. F. Hinton, P. Pulay, Efficient implementation of the gauge-independent atomic orbital method for NMR chemical shift calculations, *J. Am. Chem. Soc.* 112 (1990) 8251–8260.
- [11] E.D. Glendening, A.E. Reed, J.E. Carpenter, F. Weinhold, NBO version 3.1, TCI, University of Wisconsin, Madison, 1998.
- [12] D. Michalska, D.C. Dienko, A.J. Abkowitz-Bienko, Z. Latajka, Density Functional, Hartree–Fock, and MP2 Studies on the Vibrational Spectrum of Phenol, *J. Phys. Chem.* 100 (1996) 17786–17790.
- [13] V. Krishnakumar, V. Balachandran, T. Chithambarathanu, Density functional theory study of the FT-IR spectra of phthalimide and N-bromophthalimide, *Spectrochim. Acta* 62 (2005) 918–925.
- [14] E. Isac Paulraj, S. Muthu, Spectroscopic studies (FTIR, FT-Raman and UV), potential energy surface scan, normal coordinate analysis and NBO analysis of (2R,3R,4R,5S)-1-(2-hydroxyethyl)-2-(hydroxymethyl) piperidine-3,4,5-triol by DFT methods, *Spectrochim. Acta A* 108 (2013) 38–49.
- [15] G. Varsanyi, *Vibrational Spectra of Benzene Derivatives*, Academic Press, New York, 1969.
- [16] V. Krishnakumar, R. John Xavier, Normal coordinate analysis of 2-mercapto and 4,6-dihydroxy-2-mercapto pyrimidines, *Ind. J. Pure Appl. Phys.* 41 (2003) 597–601.
- [17] N. Sundaraganesan, H. Saleem, S. Mohan, M. Ramalingam, V. Sethuraman, FTIR, FT-Raman spectra and ab initio DFT vibrational analysis of 2-bromo-4-methylphenylamine, *Spectrochim. Acta A* 62 (2005) 740–751.
- [18] P.S. Kalsi, *Spectroscopy of Organic Compounds*, Wiley Eastern Limited, New Delhi, (1993) 116.
- [19] V. Krishnakumar, N. Prabavathi, Simulation of IR and Raman spectral based on scaled DFT force fields: A case study of 2-amino 4-hydroxy 6-trifluoromethylpyrimidine, with emphasis on band assignment, *Spectrochim. Acta A* 71 (2008) 449–457.
- [20] A. Altun, K. Golcuk, M. Kumru, Structure and vibrational spectra of p-methylaniline: Hartree-Fock, MP2 and density functional theory studies, *J. Mol. Struct. (Theochem.)* 637 (2003) 155–169.
- [21] Y.X. Sun, Q.L. Hao, Z.X. Yu, W.J. Jiang, L.D. Lu, X. Wang, Experimental and theoretical studies on vibrational spectra of 4-(2-furanylmethyleneamino)antipyrine, 4-benzylideneaminoantipyrine and 4-cinnamylideneaminoantipyrine, *Spectrochim. Acta A* 73 (2009) 892–901.
- [22] N. Sundaraganesan, B.D. Joshua, T. Radjakoumar, Molecular structure and vibrational spectra of 2-chlorobenzoic acid by density functional theory and ab-initio Hartree-Fock calculations, *Ind. J. Pure Appl. Phys.* 47 (2009) 248–258.
- [23] C. Surisseau, P. Marvel, Optical and resonance Raman scattering study of two ‘bisazo’ pigments derived from substituted benzene-2'-azonaphthols, *J. Raman Spectros.* 25 (1994) 477–488.
- [24] E. Isac Paulraj, S. Muthu, Molecular structure analysis and spectroscopic characterization of 5-ethyl-5-phenyl-1,3-diazinane-4,6-dione with experimental 4 (FT-IR and FT-Raman) techniques and quantum chemical calculations, *Spectrochim. Acta A* 106 (2013) 310–320.
- [25] R.L. Peesole, L.D. Shield, I.C. McWilliam, *Modern Methods of Chemical Analysis*, Wiley, New York, 1976.
- [26] G. Socrates, *Infrared and Raman Characteristic Group Frequencies-Tables and Charts*, third ed., Wiley, Chichester, 2001.
- [27] H.O. Kalinowski, S. Berger, S. Barun, *C-13 NMR Spectroscopy*, John Wiley and Sons, Chichester, 1988.
- [28] K. Pihlaja, E. Kleinpeter (Eds.), *Carbon-13 Chemical Shifts in Structural and Stereo Chemical Analysis*, VCH Publishers, Deerfield Beach, FL, 1994.
- [29] L.J. Pejov, M. Trpkovska, B.S. Optrajanov, Tetrafluoroberrylate(2) Ions as Hydrogen-Bond Proton Acceptors: Quantum Chemical Considerations, *Spectrosc. Lett.* 32 (1999) 361–369.
- [30] I.G. Binev, Y.I. Binev, Stamboliyska ba, Juchnovski, IR-spectra and structure of benzylidenemalononitrile and its cyanide, methoxide and heptylamine adducts - experimental and ab-initio studies, *J. Mol. Struct.* 435 (1997) 235–245.
- [31] M. Snehathatha, C. Ravikumar, I.H. Joe, N. Sekar, V.S. Jayakumar, Spectroscopic analysis and DFT calculations of a food additive Carmoisine, *Spectrochim. Acta A* 72 (2009) 654–662.
- [32] H.W. Thomson, P. Torkington, The Vibrational spectra of Esters and Ketones, *J. Chem. Soc.* 171 (1945) 640–645.
- [33] E.D. Glendening, J.K. Badenhoop, A.E. Reed, J.E. Carpenter, J.A. Bohmann, C.M. Morales, F. Weinhold, NBO 5.0, Theoretical Chemistry Institute, University of Wisconsin, Madison, 2001.
- [34] Y.R. Shen, *The Principles of Nonlinear Optics*, Wiley, New York, 1984.
- [35] C. Adant, M. Dupuis, J. L. Bredas, Ab initio study of the nonlinear optical properties of urea: Electron correlation and dispersion effects, *Int. J. Quantum Chem.* 56 (1995) 497–507.
- [36] M. Chen, U.V. Waghmare, C.M. Friend, E. Kaxiras, A density functional study of clean and hydrogen-covered MoO₃(010) Electronic structure and surface relaxation, *J. Chem. Phys.* 109 (1998) 6854–6860.
- [37] K. Fukui, Role of frontier orbitals in chemical reactions, *Science* 218 (1982) 747–754.
- [38] C.M. Breneman, K.B. Wiberg, Determining atom-centered monopoles from molecular electrostatic potentials. The need for high sampling density in formamide conformational analysis, *J. Comput. Chem.* 11(3) (1990) 361–373.
- [39] F. Jensen *Introduction to computational chemistry*, 2nd edn. Wiley-Blackwell, London, 2006.
- [40] C.J. Cramer *Essentials of computational chemistry: theories and models*, 2nd edn. Wiley, London, 2004.

- [40] P. Politzer, R.G. Parr, Some new energy formulas for atoms and molecules, *J. Chem. Phys.* 61 (1974) 4258–4262.
- [41] H. Weinstein, P. Politzer, S. Srebrenik, A misconception concerning the electronic density distribution of an atom, *Theor. Chim. Acta* 38 (1975) 159–163.
- [42] R.G. Parr, W. Yang, *Density-functional theory of atoms and molecules*. Oxford University Press, New York, 1989.
- [43] P. Politzer, In *homo atomic rings, chains and macromolecules of main-group elements*. Elsevier, Amsterdam, 1977.
- [44] P. Sjöberg, P. Politzer, Use of the electrostatic potential at the molecular surface to interpret and predict nucleophilic processes, *J. Phys. Chem.* 94 (1990) 3959–3961.
- [45] R.K. Roy, S. Krishnamurti, P. Geerling, S. Pal, Local Softness and Hardness Based Reactivity Descriptors for Predicting Intra- and Intermolecular Reactivity Sequences: Carbonyl Compounds, *J. Phys. Chem A* 102 (1998) 3746–3755.
- [46] R. Parthasarathi, V. Subramanian, D.R. Roy, P.K. Chattaraj, Electrophilicity index as a possible descriptor of Biological activity, *Bioorg. Med. Chem.* 12 (2004) 5533–5543.
- [47] M. A. Spackman, J. J. McKinnon, Fingerprinting intermolecular interactions in molecular crystals, *Cryst. Eng. Comm.* 4 (2002) 378–392.
- [48] J. J. McKinnon, F. P. A. Fabbiani, M. A. Spackman, Comparison of polymorphic molecular crystal structures through Hirshfeld surface analysis *Cryst. Growth Des.* 7 (2007) 755–769.
- [49] J. J. McKinnon, D. Jayatilaka, M. A. Spackman, Towards quantitative analysis of intermolecular interactions with Hirshfeld surfaces, *Chem. Commun.* 37 (2007) 3814–3816.
- [50] J. J. McKinnon, M. A. Spackman, A. S. Mitchell, Novel tools for visualizing and exploring intermolecular interactions in molecular crystals, *Acta Crystallogr. Sect. B: Struct. Sci.* 60 (2004) 627–638.
- [51] D. Gfeller, A. Grosdidier, V. Zoete, Swisstarget prediction: A web server for target prediction of bioactive small molecules, *Nucl. Acids Res.* 42(W1) (2014) W32–W38.
- [52] D. Gfeller, O. Michielin, V. Zoete, Shaping the interaction landscape of bioactive molecules, *Bioinformatics* 29(23) (2013) 3073–3079.
- [53] A.L. Morris, M.W. MacArthur, E.G. Hutchinson, Stereochemical quality of protein structure coordinates, *J.M. Thornton, Proteins*, 12 (1992) 345–364.
- [54] O. Trott, A. J. Olson, Software news and update AutoDock Vina: Improving the speed and accuracy of docking with a new scoring function, efficient optimization, and multithreading, *J. Comput. Chem.* 31(2010) 455–461.
- [55] X. Tan, L.I.A. Calderon-Villalobos, M. Sharon, C. Zheng, C.V. Robinson, M. Estelle, N. Zheng, Mechanism of auxin perception by the TIR1 ubiquitin ligase, *Nature*. 446 (2007) 640–645.
- [56] M. Sugishima, Y. Hagiwara, X. Zhang, T. Yoshida, C.T. Migita, K. Fukuyama, Crystal Structure of Dimeric Heme Oxygenase-2 from *Synechocystis* sp. PCC 6803 in Complex with Heme, *Biochemistry* 44 (2005) 4257–4266.